AIAA SciTech Forum
9 - 13 January 2017, Grapevine, Texas
19th AIAA Non-Deterministic Approaches Conference

Efficient Global Sensitivity Analysis for Time-Dependent, Multidisciplinary Models

Erin C. DeCarlo[1] and Sankaran Mahadevan[2]
Vanderbilt University, Nashville, TN, 37235

Benjamin P. Smarslok[3] and Daniel M. Sparkman[4]
Air Force Research Laboratory, Wright-Patterson AFB, OH, 45433

This paper presents methodology for efficiently computing global sensitivity indices for time-dependent, coupled analyses. First, the developed methods increase the efficiency of the pre-calibration sensitivity computation by incorporating optimal space-filling quasi-random sequences into an existing importance sampling-based kernel regression sensitivity method. Next, the sensitivity methodology is generalized for correlated quantities which occur in posterior parameter distributions, as well as in coupled analyses through time. The post-calibration sensitivity analysis is performed without requiring additional model evaluations by efficiently using input-output relationships obtained from Bayesian calibration. The methodology is used to estimate post-calibration sensitivities of coupled aerothermal models through time. It is observed that model errors and parameter correlations control the sensitivity estimates until coupling effects become dominant.

Nomenclature

D	=	dimension of input space
h	=	bandwidth of Gaussian kernel
K	=	kernel function
M	=	number of model evaluations
N	=	number of sensitivity iterations
p	=	probability density function
Q	=	heat flux (W/m^2)
$S_{d,1}$	=	first-order effect of parameter X^d
$S_{d,T}$	=	total effect of parameter X^d
t	=	time
T	=	temperature (K)
x	=	model input
X^d	=	samples for d^{th} input dimension
$\boldsymbol{X}^{\sim d}$	=	samples for all but d^{th} input dimension
y	=	model output
Y	=	vector of M model outputs
δ	=	aerothermal model discrepancy
ε	=	model discrepancy
Δt	=	time step
θ	=	model parameter
μ	=	mean
σ^2	=	variance

[1] Ph.D Candidate, Dept. of Civil & Environmental Engineering, AIAA Member, erin.c.decarlo@vanderbilt.edu
[2] John. R. Murray Sr. Professor of Engineering, Dept. of Civil & Environmental Engineering, AIAA Associate Fellow
[3] Research Aerospace Engineer, Aerospace Systems Directorate, Structural Sciences Center, AIAA Member
[4] Research Mechanical Engineer, Materials and Manufacturing Directorate, AIAA Member.

Subscripts

0	=	initial condition
1	=	1st model in a series
2	=	2nd model in a series
4	=	panel location
d	=	input dimension index
f	=	final time of interest
i	=	i^{th} outer-loop sensitivity iteration
j	=	j^{th} model evaluation or inner-loop sensitivity iteration
t	=	time index
X^d	=	statistic of X^d
$\boldsymbol{X}^{\sim d}$	=	statistic of $\boldsymbol{X}^{\sim d}$

Superscripts

d	=	d^{th} input dimension

I. Introduction

AIRCRAFT structures subjected to extreme hypersonic environments exhibit highly coupled, multi-physics, fluid-thermal-structural (aerothermoelastic) response. Accurately predicting these complex fluid-thermal-structural interactions is a significant and important challenge that must be overcome for the US Air Force to field a reusable, air-breathing hypersonic aircraft. Uncertainty inherently exists within models from each discipline due to imperfect knowledge, numerical errors, solution approximation errors, and model discrepancy [1]. Additionally, the coupled interactions between the multidisciplinary models also introduce uncertainty during the long duration simulation.

Several recent research efforts have focused on investigating the model components for the physics of a coupled aerothermoelastic panel [2–10]. However, the current state of the art focuses on deterministic calculations with limited uncertainty analysis. Lamorte et al. investigated the implementation of a stochastic collocation approach for propagating uncertainty in aerothermoelastic analysis [11]. Related work expanded on uncertainty propagation in aerothermoelastic analysis for hypersonic vehicles with emphasis on assessing the impact of aerothermoelastic deformation on aerodynamic heating [12]. Culler et al. also identified two-way coupling between structural deformation and aerodynamic heating as an important consideration in modeling an aerothermoelastic panel [13]. These efforts underscore the importance of understanding uncertainty in coupled aerothermoelastic models and its downstream effects on prediction confidence through a global sensitivity analysis.

Sensitivity analyses provide insight on how the system is influenced by a given parameter across the problem domain. In contrast to gradient-based local sensitivities at a chosen nominal value, global sensitivity analysis (GSA) uses parameter probability information and quantifies both the individual and interactive effects between the various uncertainty sources on the model output. This is especially important in a multidisciplinary model calibration where many uncertain and interrelated parameters and model outputs are present [14].

Sampling-based sensitivity estimation uses random samples (e.g., Monte Carlo simulation (MCS)) of input-output data to estimate the first-order and total effects of uncertain parameters. When the sensitivity indices are computed using the standard method consisting of a nested Monte Carlo sampling loop, the number of model runs increases to $O(2kN^2)$, where N is the number of samples in the inner loop MCS, and k is the number of variables. Saltelli's widely-used class of matrix column-exchange methods [15] improve the cost to $O(N(k+2))$ however, are still intractable when sensitivities through time are of interest for coupled problems.

To alleviate the cost of repeated evaluations of expensive models, surrogate models are often used in place of the actual simulation [16,17]; however, the additional step of training and assessing the reliability of the surrogate across adequately across input probability space requires sufficient model evaluations and surrogate model error becomes another uncertainty source. Furthermore, surrogate modeling of the individual disciplines in a multidisciplinary analyses that iterate through time is challenging [18,19]. Therefore, post-processing an established set of input-output data from the model development, calibration, and validation stages using nonparametric methods [20,21] is explored.

First, the proposed methodology builds from a post-processing importance sampling-based kernel method for estimation of the Sobol' indices (ISK-GSA) developed by Sparkman et. al. [21]. The ISK-GSA method calculates Sobol' indices in fewer model runs using additional importance sampling-based weights and kernel regression estimate of the conditional means used for Sobol' sensitivity indices. Furthermore, studies have found that quasi-random sequences provide optimal space-filling designs in higher dimensions [22]. The combined methodologies and the specific usefulness in efficiently assessing pre-calibration sensitivities of a single discipline model across a wide

range of its inputs are detailed further in this paper. Second, the ISK-GSA method is generalized to allow consideration of correlated quantities which are observed a) in posterior samples of calibrated parameters and b) multidisciplinary model predictions and errors through time. With the generalized ISK-GSA methodology developed herein, a greater understanding of the interactions between models, their errors, and correlated parameters through time is achieved.

Sobol' sensitivity indices for global sensitivity analyses are given in Section II.A followed by an overview of the ISK-GSA method as developed by Sparkman et Al. presented in Section II.B. Section III first presents the methodology suitable for pre-calibration sensitivity analysis that uses space-filling quasi-random number generators with the ISK-GSA. Next, the generalized ISK-GSA formulation is developed to handle correlated quantities observed in both post-calibration and between coupled models through time, which is then demonstrated on an illustrative time-dependent example. Section IV applies generalized ISK-GSA methodology to calibrated aerothermal models for a posterior global sensitivity analysis through time and demonstrates the effects of model coupling and parameter correlation on the time-dependent sensitivity estimates.

II. Global Sensitivity Analysis Methodology

Sobol' sensitivity indices for global sensitivity analysis (GSA) are presented in Section II.A followed by an efficient post-processing importance sampling-based kernel regression method for computing the Sobol' indices (ISK-GSA) in Section II.B. An analytical two-dimensional example demonstrating that few model evaluations are needed for ISK-GSA compared to double-loop (DL) and matrix column exchange (MCE) methods for GSA is presented in Section II.C.

A. Sobol' Sensitivity Indices

Based on the variance decomposition theorem in Eq. (1) the total variance $Var(Y)$ in model output Y from D-dimensional uncertain parameter vector $\boldsymbol{X}$ can be decomposed into two parts: 1) the variance of $E_{\boldsymbol{X}_{\sim d}}[Y|X^d]$, that is the conditional expectation of model output Y given parameter X^d (d = 1 to D) with all other parameters $\boldsymbol{X}^{\sim d}$ varying; and 2) the expectation of $Var_{\boldsymbol{X}_{\sim d}}[Y|X^d]$, that is the variance of Y conditioned the same the same set [15,23].

$$Var(Y) = Var_{X^d}\{E_{\boldsymbol{X}^{\sim d}}[Y \mid X^d]\} + E_{X^d}\{Var_{\boldsymbol{X}^{\sim d}}[Y \mid X^d]\} \tag{1}$$

The two quantities of interest in GSA are the first-order and total effect indices of each parameter X^d on model output Y. The first-order Sobol' index $S_{d,1}$ is the ratio of variance X^d contributes to the total variance $Var(Y)$ shown in Eq. (2) and is estimated using the variance of the conditional expectation $E_{\boldsymbol{X}_{\sim d}}[Y|X^d]$ in the numerator. The sum of the first-order indices across all D dimensions is equal to 1 (within a margin of finite sampling error), or less than 1 if parameter interactions are significant.

$$S_{d,1} = \frac{Var_{X^d}\{E_{\boldsymbol{X}^{\sim d}}[Y \mid X^d]\}}{Var(Y)} \tag{2}$$

The total effects Sobol' index $S_{d,T}$ in Eq. (3) represents both the first-order effects of X^d and interaction effects between parameters X^d and $\boldsymbol{X}^{\sim d}$ that are not captured by the first-order Sobol' index. The total effects in Eq. (3) are derived by dividing the second term in the variance decomposition shown in Eq. (1) by $Var(Y)$. Therefore, for any two parameter sets X^d and $\boldsymbol{X}^{\sim d}$ both $S_{\sim d,T} = 1 - S_{d,\underline{1}}$ and $S_{d,\underline{T}} = 1 - S_{\sim d,1}$ are true. Rearranging, the second part of Eq. (3) is obtained for the total effects Sobol' index $S_{d,T}$.

$$S_{d,T} = \frac{E_{\boldsymbol{X}^{\sim d}}\{Var_{\boldsymbol{X}^d}[Y \mid X^{\sim d}]\}}{Var(Y)} = 1 - \frac{Var_{\boldsymbol{X}^{\sim d}}\{E_{X^d}[Y \mid \boldsymbol{X}^{\sim d}]\}}{Var(Y)} \tag{3}$$

A nested double-loop (DL) algorithm was proposed to compute the indices. A double-loop computation of the first-order Sobol' index for parameter X^d first consists of an outer-loop at fixed $X^d = x_i^d$ (i = 1 to N_{outer}), and an inner-loop over $\boldsymbol{X}^{\sim d} = \boldsymbol{x}_j^{\sim d}$ (j = 1 to N_{inner}) computes the conditional expectation estimate $E_{\boldsymbol{X}_{\sim d}}[Y|X^d = x_i^d]$. This process is repeated over all N_{outer} outer-loop iterations, where the variance of the estimates of $E_{\boldsymbol{X}_{\sim d}}[Y|X^d = x_i^d]$ (i = 1 to N_{outer}) composes the numerator of Eq. (2). Considering $N_{outer} = N_{inner} = N$, the number of model evaluations M needed to compute both the first-order and total effect Sobol' indices for each of D parameters is $M \sim O(2DN^2)$).

Matrix-column exchange (MCE) methods first explored by Saltelli et al. [15] decreased the computational expense of computing the Sobol' sensitivity indices by directly estimating the variances of the numerators in Eqs. (2) and (3). First, MCE methods require a *2N*x*D* design of computer experiments $\boldsymbol{X}$ which is sub-divided into two *N*x*D* matrices $\boldsymbol{X}_A$ and $\boldsymbol{X}_B$ that lead to outputs y_A and y_B and the number of model evaluations $M \sim O(2(2+D)N)$. A matrix $\boldsymbol{X}_{AB}{}^d$ for each dimension d is then formed by permuting the d^{th} column of $\boldsymbol{X}_A$ with $\boldsymbol{X}_B{}^d$ leading to $y_{AB}{}^d$ for d = 1 to D and likewise for $\boldsymbol{X}_{BA}{}^d$ and $y_{BA}{}^d$. The improved MCE variances from [24] are presented below in Eqs. (4) and (5).

$$Var_{X^d}\{E_{\boldsymbol{X}^{\sim d}}[Y \mid X^d]\} = \frac{1}{N-1}\sum_{n=1}^{N} y_{A,n} y_{BA,n}^d - \frac{1}{N}\sum_{n=1}^{N} y_{A,n} y_{B,n} \tag{4}$$

$$Var_{\boldsymbol{X}^{\sim d}}\{E_{X^d}[Y \mid \boldsymbol{X}^{\sim d}]\} = \frac{1}{N-1}\sum_{n=1}^{N} y_{A,n} y_{AB,n}^d - \frac{1}{N}\sum_{n=1}^{N} (y_{A,n})^2 \tag{5}$$

The challenge with computing Sobol' indices for time-dependent, multidisciplinary analyses with either the DL or MCE methods is two-fold; 1) convergence of the sensitivity estimate is slow from sub-optimal sampling and expensive models, and 2) MCE methods are unable to accommodate correlated quantities. First, computational challenges addressed using ISK-GSA in its original form and improved upon in Section II.A using Sobol' sequences. Performing sensitivity analyses for coupled models and correlated parameters is addressed in Section III.

B. Importance Sampling-based Kernel Regression Estimator for Sobol' Indices (ISK-GSA)

The proposed methodology found in Section III is dependent on the formulation of the ISK-GSA method developed by Sparkman et al. [21]. This section first introduces the independent concepts of kernel regression and importance sampling and how they combine for estimating sensitivities using ISK-GSA. Then the ISK-GSA methodology is compared against DL and MCE methods for a simple example to demonstrate the computational savings offered and to serve as a basis for comparing the generalized ISK-GSA methodology for correlated variables in Section III.

Consider *M* available model evaluations from various stages of model development with input-output relationships X_{MxD} and Y_{Mx1}. For each model evaluation m = 1 to M and input dimension d = 1 to D, an estimate of the conditional expectation $E_{X\sim d}[Y \mid X^d = x_m{}^d]$ is achieved by a selective weighting of the M model outputs Y as shown in Eq. (6). Kernel regression, importance sampling, and ISK-GSA estimates differ how the normalized weights $w_j{}^d$ are computed, as shown in Eqs. (7)-(9).

$$E_{X^{\sim d}}[Y \mid X^d = x_m^d] = \sum_{j=1}^{M} y_j w_j^d \tag{6}$$

Kernel regression for the conditional expectation in Eq. **Error! Reference source not found.** uses a locally weighted average of output samples of Y in the neighborhood of $x_m{}^d$. The neighborhood is defined by a kernel $K_d(x_m{}^d - x_j{}^d)$ centered around on $x_m{}^d$ and the normalized weights $w_j{}^d$ for kernel regression are defined according to Eq. (7).

$$w_j^d = \frac{K_d(x_m^d - x_j^d)}{\sum_{j=1}^{M} K_d(x_m^d - x_j^d)} \quad \text{[Kernel regression weights]} \tag{7}$$

Importance sampling is a variance reduction technique that distinguishes a sampling density (i.e., the joint probability density of the input space $S_D(\boldsymbol{x})$) where model evaluations M have occurred and a target density (i.e., the joint probability density $T_D(\boldsymbol{x})$ where statistics are desired). For each input dimension d from 1 to D, the estimate of an output statistic for target distribution $T_d(x^d)$ using samples from the sampling density $S_d(x^d)$ is achieved using normalized importance-sampling weights $w_j{}^d$ defined according to Eq. (8).

$$w_j^d = \frac{T_d(x_j^d)/S_d(x_j^d)}{\sum_{j=1}^{M} T_d(x_j^d)/S_d(x_j^d)} \quad \text{[Importance sampling weights]} \tag{8}$$

The formulation for the ISK-GSA estimate weights arises out of equating the kernel $K_d(x_m^d - x_j^d)$ that defines the neighborhood around x_m^d and the marginal target density $T_d(\mathbf{x})$. Likewise, and the sampling density $S_d(x^d)$ is the marginal probability density of the available inputs $p_d(x^d)$ in each input dimension. Thus, for each model evaluation M, the conditional expectation in Eq. **Error! Reference source not found.** for first order effects is estimated using the ISK weights in Eq. (9).

$$w_j^d = \frac{K_d(x_m^d - x_j^d) / p_d(x_j^d)}{\sum_{j=1}^{M} K_d(x_m^d - x_j^d) / p_d(x_j^d)} \quad \text{[First order index weights for ISK-GSA]} \tag{9}$$

The conditional expectations for total effects indices in Eq. (3) for the ISK-GSA estimates are computed similarly with multidimensional kernel $K_{\sim d}(\mathbf{x}_m^{\sim d} - \mathbf{x}_j^{\sim d})$ defining the neighborhood around $\mathbf{x}_m^{\sim d}$ and joint probability density $p_{\sim d}(\mathbf{x}_m^{\sim d})$ in Eqs. (10) and (11). The weight formulation in Eq. (11) assumes that the d and $\sim d$ kernels and probability distributions are independent.

$$E_{X^d}[Y \mid X^{\sim d} = x_m^{\sim d}] = \sum_{j=1}^{M} y_j w_j^{\sim d} \tag{10}$$

$$w_j^{\sim d} = \frac{K_{\sim d}(x_m^{\sim d} - x_j^{\sim d}) / p_{\sim d}(x_j^{\sim d})}{\sum_{j=1}^{M} K_{\sim d}(x_m^{\sim d} - x_j^{d}) / p_{\sim d}(x_j^{\sim d})} \quad \text{[Total index weights for ISK-GSA]} \tag{11}$$

In this work, Gaussian kernels are used and the sampling distribution of each X^d is Gaussian with mean μ_d and standard deviation σ_d. Thus the kernel bandwidths h_d in each dimension were assumed to be $1.06\sigma_d M^{-1/5}$, as suggested for Gaussian kernels in [21]. Thus, the kernel bandwidth in each dimension scales to the sampling variance σ_d and decreases as the number of model evaluations M.

To demonstrate the computational benefits of the ISK-GSA methodology for sensitivity analysis, consider a two-parameter model $y = 2x_1 + x_2$ where both parameters are considered independent Gaussian random variables with zero mean and unit variance. The first order and total effect Sobol' indices for each parameter are equivalent indicated by Eqs. (8) and (9) due to no parameter interactions or correlations. The true sensitivities of y to x_1 and x_2 are 0.8 and 0.2, respectively. Figure 1 compares sensitivity estimates using latin-hypercube sampling (LHS) for double-loop (DL), Saltelli's matrix column-exchange method (MCE), and the ISK-GSA method from N = 1 to 400 and D = 2.

$$S_{x_1,1} = S_{x_1,T} = \frac{Var_{x_1}\{E_{x_2}[y \mid x_1]\}}{Var(y)} = \frac{4\sigma_{x1}^2}{4\sigma_{x1}^2 + \sigma_{x2}^2} \tag{12}$$

$$S_{x_2,1} = S_{x_2,T} = \frac{Var_{x_2}\{E_{x_1}[y \mid \theta_2]\}}{Var(y)} = \frac{\sigma_2^2}{c^2\sigma_1^2 + \sigma_2^2} \tag{13}$$

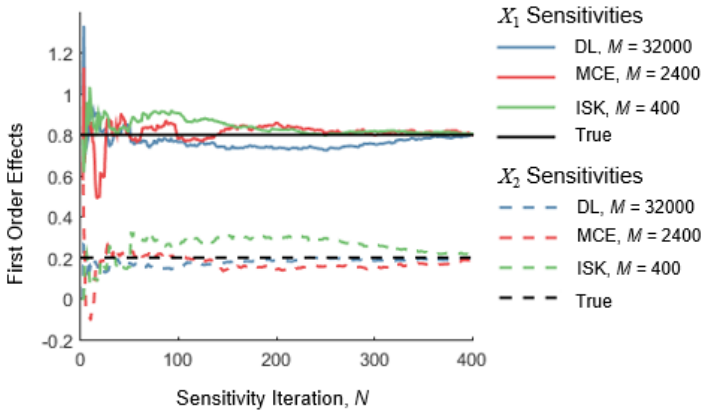

Figure 1. First order effects of x_1 (top) and x_2 (bottom) across N sensitivity iterations

The legend in Figure 1 that indicates the number of model evaluations needed for each DL, MCE, and ISK-GSA method shows that the ISK-GSA method requires less than 1% of the model evaluations required for the DL estimate and less than 17% compared to the MCE method. The number of model evaluations to compute the first order and total effect indices for the ISK-GSA method at each sensitivity iteration N is $O(N)$ opposed to $O(2DN^2)$) and $O(2(2+D)N)$ for the DL and MCE methods, respectively.

This example will be used in Section III.A to demonstrate the proposed methodology for prior sensitivity analysis using quasi-random variables to improve upon the convergence of the ISK-GSA sensitivity estimates. Then, extension of the ISK-GSA methodology to correlated quantities is derived in Section III.B for post-calibration sensitivity analysis and for time-dependent, multidisciplinary and applied to the posterior sensitivities of coupled aerothermal models through time in Section IV.

III. Proposed Methodology

The proposed methodology extends the capability of the ISK-GSA method for estimating Sobol' sensitivity indices by pairing it with efficient sampling techniques in Section III.A. Namely, quasi-random number generators (e.g., Sobol' sequences) are investigated to replace random and pseudo-random number generators (e.g., latin hypercube designs) for design of computer experiments for global sensitivity analysis. The two-dimensional example problem from Section II is used here to demonstrate the added efficiency provided by using a Sobol' sequence.

Next, the ISK-GSA method is generalized in Section III.B to include correlated variables using joint kernels and joint probability density functions. The generalized ISK-GSA method is tested on a simple coupled, time-dependent example that highlighting the effect of correlation among model parameters.

A. Pre-Calibration ISK-GSA with Quasi- Random Number Generators

Quasi-random and pseudo-random number generators are two classes of algorithms used to generate Monte Carlo samples for numerical integration, uncertainty propagation, and sensitivity analysis. Pseudo-random number generators (e.g., latin-hypercube) have the advantages of being most random-like, as shown in the left-hand side of Fig. 2, but result in regions of high and low density. This quality is undesirable as it can prolong convergence of the integration. Quasi-random sequences were developed for efficiency in numerical integration schemes, which need even coverage over a high-dimensional integral domain [25].

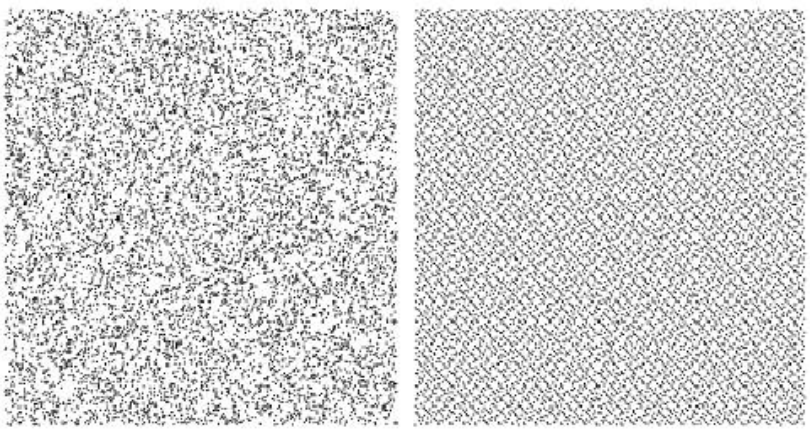

Figure 2. Latin-Hypercube design (left) and Sobol' sequence (right) with 10,000 points

A quasi-random sequence (e.g., Sobol' sequences, Halton sequences, or Hammersley sets), however, is guaranteed to cover the domain of interest evenly for fast convergence. This work makes use of the Sobol' sequence which fills the in space sequentially after each iteration N such that the difference between the domain coverage between N-1 and N iteration is low.

Again considering the model $y = 2x_1 + x_2$ from Section II.C, the advantages of using a Sobol' sequence are evident when N is constrained to a low number of model evaluations (N = 450) shown in Fig. 3. We observe the asymptotic convergence of the sensitivity estimate when a quasi-random Sobol' sequence is used with the ISK-GSA method compared to using a Sobol' sequence with the DL or MCE methods. A convergence criterion can then be applied to terminate the sensitivity analysis to minimize computational effort. One reason for this convergence using the ISK-GSA method is the decreasing kernel bandwith as M increases according to $h_d = 1.06\sigma_d M^{-1/5}$ and the sequential space-filling algorithm of the Sobol' sequence contributes to the 'stair-step' pattern of convergence in Fig. 3.

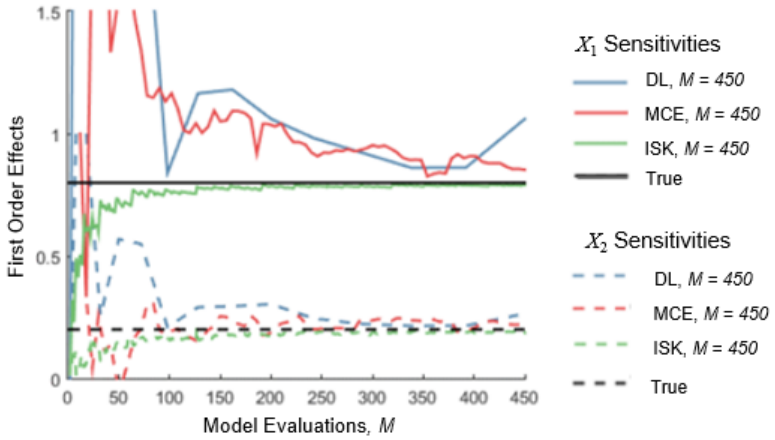

Figure 3. Comparison of x_1 and x_2 first order effects using 2D Sobol' sequence and LHS design

Pre-calibration sensitivity analysis for time-dependent, multidisciplinary models will be conducted using the ISK-GSA methodology with Sobol' sequences to reduce the number of coupled simulations required for these sensitivity estimates. Posterior sensitivity analyses with correlated posterior parameter distributions is addressed in the next section.

B. Generalized ISK-GSA with Correlated Parameters

Model calibration is performed using sampling methods (e.g., MCMC, slice sampling, or particle-filtering) which require a significant number of model evaluations until posterior convergence. The input-output relationships between the accepted posterior samples and the model output represents a database of models runs that have since remain unusable for sensitivity analysis due to induced correlation between co-calibrated parameters. In coupled model discrepancy calibration, in particular, the correlation between model errors can be close to -1 with additional cross-correlations among the calibrated error.

The formulation of the normalized weights for a generalized ISK-GSA estimate with correlated parameters involves recognizing that Eqs. (9) and (14) are equivalent for independent variables since the marginal density $p_d(x^d)$ is equivalent to the joint density $p_D(\boldsymbol{x})$ divided by $p_{\sim d}(\boldsymbol{x}^{\sim d})$ when $\boldsymbol{X}^{\sim d}$ and X^d are independent. Likewise, the marginal kernel $K_d(x_m^d - x_j^d)$ centered on $\boldsymbol{x}_m^d$ is equivalent to the joint kernel $K_D(\boldsymbol{x}_m^D - \boldsymbol{x}_j^D)$ centered on $\boldsymbol{x}_m^D$ divided by the $K_{\sim d}(\boldsymbol{x}_m^{\sim d} - \boldsymbol{x}_j^{\sim d})$ centered on $\boldsymbol{x}_m^{\sim d}$.

$$w_j^d = \frac{K_D(\boldsymbol{x}_m^D - \boldsymbol{x}_j^D)\, p_{\sim d}(\boldsymbol{x}_j^{\sim d}) / K_{\sim d}(\boldsymbol{x}_m^{\sim d} - \boldsymbol{x}_j^{\sim d})\, p_D(\boldsymbol{x}_j^D)}{\sum_{j=1}^{M} K_D(\boldsymbol{x}_m^D - \boldsymbol{x}_m^D)\, p_{\sim d}(\boldsymbol{x}_j^{\sim d}) / K_{\sim d}(\boldsymbol{x}_m^{\sim d} - \boldsymbol{x}_j^{\sim d})\, p_D(\boldsymbol{x}_j^D)} \tag{14}$$

While Eq. (14) reduces to Eq. (9) for independent variables, Eq. (15) demonstrates the generalized ISK-GSA weight for first-order effects in Eq. **Error! Reference source not found.** where X^d and $\boldsymbol{X}^{\sim d}$ need not be independent. In Eq. (15), both the kernel defining the neighborhood around x_m^d and probability of x_j^d are conditioned on $x_m^{\sim d}$. If there is no dependence between X^d and $\boldsymbol{X}^{\sim d}$ then $p_{d|\sim d}(x^d|\boldsymbol{x}^{\sim d}) = p_d(x^d)$ and $K_{d|\sim d}(x^d|\boldsymbol{x}^{\sim d}) = K_d(x^d)$ and Eq. (15) reduces to Eq. (9).

$$w_j^d = \frac{K_{d|\sim d}(x_m^d - x_j^d \mid X^{\sim d} = x_m^{\sim d}) / \, p_{d|\sim d}(x_j^d \mid X^{\sim d} = x_m^{\sim d})}{\sum_{j=1}^{M} K_{d|\sim d}(x_m^d - x_j^d \mid X^{\sim d} = x_m^{\sim d}) / \, p_{d|\sim d}(x_j^d \mid X^{\sim d} = x_m^{\sim d})} \tag{15}$$

For completeness, the generalized ISK-GSA weights for total effects are presented in Eq. (16) and are equivalent to Eq. (11) when X^d and $\boldsymbol{X}^{\sim d}$ are independent.

$$w_j^{\sim d} = \frac{K_{\sim d|d}(x_m^{\sim d} - x_j^{\sim d} \mid X^d = x_m^d) / \, p_{\sim d|d}(x_j^{\sim d} \mid X^d = x_m^d)}{\sum_{j=1}^{M} K_{\sim d|d}(x_m^{\sim d} - x_j^{\sim d} \mid X^d = x_m^d) / \, p_{\sim d|d}(x_j^{\sim d} \mid X^d = x_m^d)} \tag{16}$$

The generalized ISK=GSA methodology is first demonstrated on an example problem to illustrate models with a time-dependent, coupled relationship and then used for post-calibration sensitivity analysis of coupled aerothermal models in Section IV.

C. Time-Dependent, Multidisciplinary Example with Correlated Parameters

Consider the coupled models in Eq. (17) that are representative of multidisciplinary, time dependent analyses. The models are coupled such that one model output feeds into the next where 1) the value of model output y_1 moves from 1 toward zero through time as y_2 grows from initial condition $y_{2,0}$ and 2) y_2 advances from initial condition $y_{2,0}$ at a rate of $y_{1,I}$ across $\Delta t = 0.1s$ until the final time of interest $t_f = 50s$.

$$\begin{aligned} y_{1,i} &= \frac{y_{2,0}}{y_{2,i-1}} + \varepsilon_1 \\ y_{2,i+1} &= y_{2,i} + y_{1,i}\Delta t + \varepsilon_2 \end{aligned} \tag{17}$$

Three sources of uncertainty are considered for global sensitivity analysis and propagated through the coupled system; uncertain model errors (ε_1, ε_2) and the initial condition $y_{2,0}$ which are first considered as independent Gaussian

random variables with statistics shown in Table 1 and a then considered to have the correlation structure shown in Eq. (18) where ρ_{23} = -0.5 is the negative correlation between model errors ε_1 and ε_2.

Table 1. Model parameters for time-dependent example

Parameter	Mean	Variance
$y_{2,0}$	20	4
ε_1	0	4e-4
ε_2	0	4e-4

$$\rho = \begin{bmatrix} 1 & 0 & 0 \\ 0 & 1 & -0.5 \\ 0 & -0.5 & 1 \end{bmatrix} \tag{18}$$

A three-dimensional Sobol' sequence was generated for $y_{2,0}$, ε_1, ε_2 and propagated through to model outputs y_1 and y_2 until t_f = 50s. Figure 4 demonstrates the prediction uncertainty in both y_1 and y_2 when just the uncertainty in the input condition is propagated as a random variable (RV) with ε_1 and ε_2 fixed at their mean values (black), when all three sources of uncertainty are propagated as RVs (blue), and when correlation among ε_1 and ε_2 is considered (green). Note that since ε_1 and ε_2 both have zero mean, the mean predictions overlap for each of the three cases shown in Figs. 4a and 4b. Also, a negative correlation between ε_1 and ε_2 slightly increases uncertainty in y_1 predictions but decreases the uncertainty in y_2.

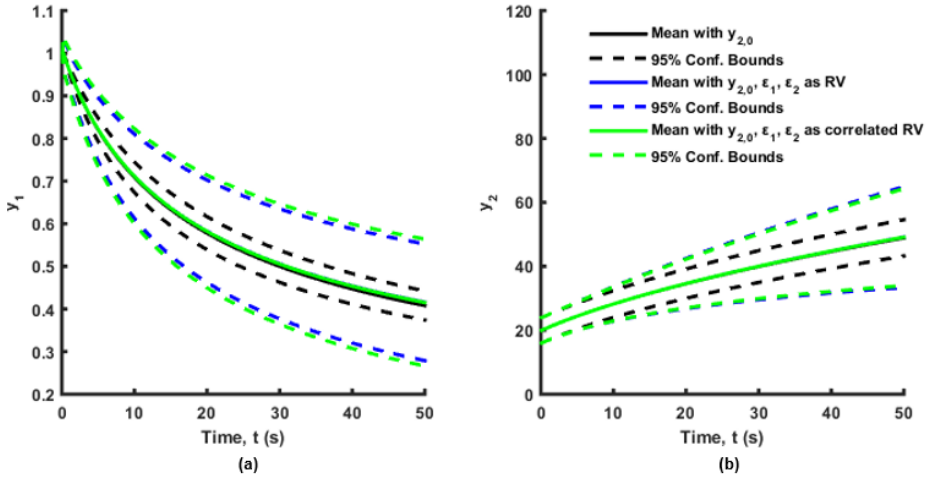

Figure 4. Coupled y_1 predictions (a) and y_2 predictions (b) through t = 50s

The sensitivities throughout the time to $y_{2,0}$, ε_1, and ε_2 for each model were computed using the generalized ISK-GSA methodology for both the correlated and uncorrelated parameter cases. The first-order (Eqs. (6) and (15)) and the total effects Sobol' indices (Eqs. (10) and (16)) were computed with a 3-dimensional Sobol' sequence of N = 1,000(15) which was assumed to be the conditional cumulative density function (CDF) values in each dimension d.

The first-order effects and total effects for y_1 for the independent and correlated cases are shown in Fig. 5 where both ISK-GSA estimates adhere to the summation criterion of $\Sigma S_{d,1} \leq 1$ for the first-order indices in Figs. 5a and 5c and $\Sigma S_{d,T} \geq 1$ for the total effects in Figs. 5b and 5d. The first-order and total effects on y_1 for the independent parameter case (Fig. 5a-b) are equivalent. This indicates that there are no inherent parameter interactions within the model itself that contribute additional sources of uncertainty. The sensitivity of y_1 to initial condition $y_{2,0}$ decreases over time as expected, however, there is a trade-off between y_1 sensitivity to ε_1 and ε_2 since the model output becomes more influenced by ε_2 as more coupled iterations occur through time.

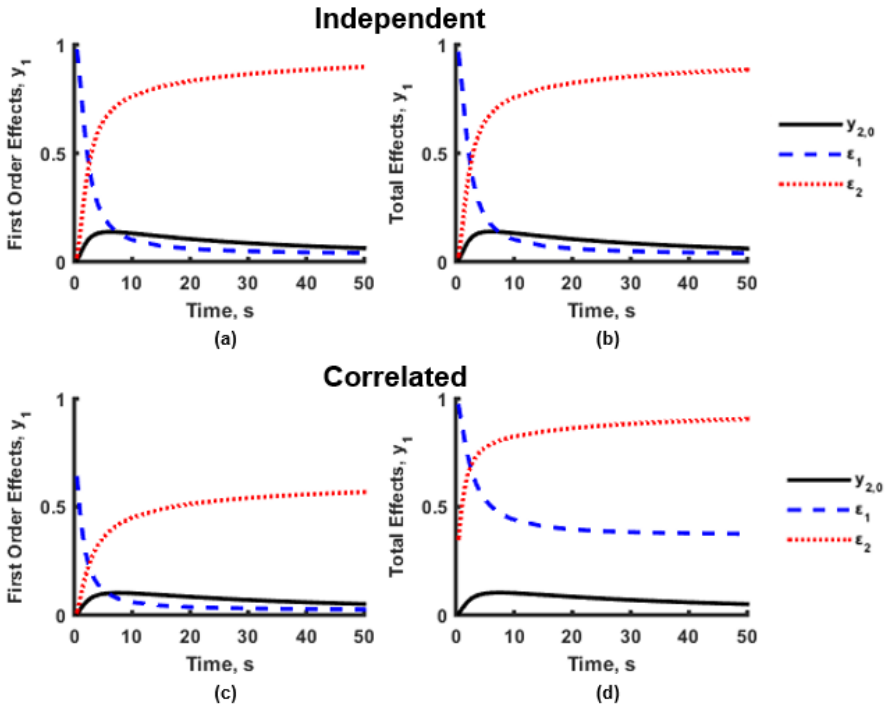

Figure 5. First-order and total effects on model output y_1 with independent (top) and correlated (bottom) parameters

Figures 5c-d also the individual first-order effects ε_1 and ε_2 decrease when correlation is considered between ε_1 and ε_2 across all time instances. This is intuitive since the total effects capture parameter interactions regardless of their source. In addition, correlation between ε_1 and ε_2 has negligible effects either the first-order or total effects of $y_{2,0}$ on y_1 in either the independent and correlated cases.

The same conclusions are similarly drawn from Fig. 6 showing the sensitivity indices for y_2 where 1) the first-order sensitivities in Fig. 6a and total effect indices in Fig. 6b are equivalent in the independent case due to negligible parameter interactions within the models themselves and 2) y_2 sensitivity to $y_{2,0}$ undergoes little change between the independent and correlated cases. Furthermore, the first-order effects of ε_1 on y_2 in Fig. 6c with correlation are similar to the independent case and sum close to unity because the sensitivity of y_2 to ε_1 is low. The effect of correlation between ε_1 and ε_2 on the output y_2 is only apparent in the total effects of y_2 in Fig. 6d.

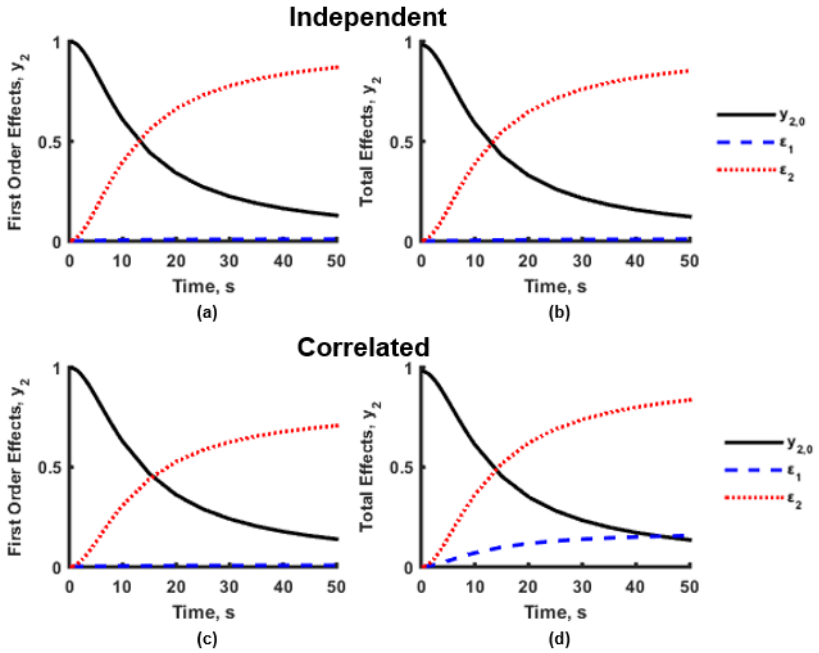

Figure 6. Sensitivities of model output y_2 with independent (a-b) and correlated (c-d) parameters

With correlations between ε_1 and ε_2 ranging from -0.9 to 0.9 in Fig. 7, the effects of positive and negative correlation on both y_1 and y_2 sensitivities to model error ε_2 are observed. A positive correlation between ε_1 and ε_2 of 0.5 or 0.9 leads to initial first-order effects of ε_2 that are greater than the total effects on y_1. The inverse relationship between $y_{1,t}$ and $y_{2,t}$ along with a positive correlation between their errors results in an initial decrease in the prediction uncertainty of y_1 that grows after t = 5s. Shown by the red and blue dotted lines in Figs. 7a-b, the effects of positive correlation become damped out as ε_2 begins to dominate the y_1 prediction and is expedited by the degree of positive correlation. The effects observed with positive correlation in Figs. 7a-b are not seen in the negative correlation cases cases since the uncertainty in y_1 monotonically increases over the entire time history.

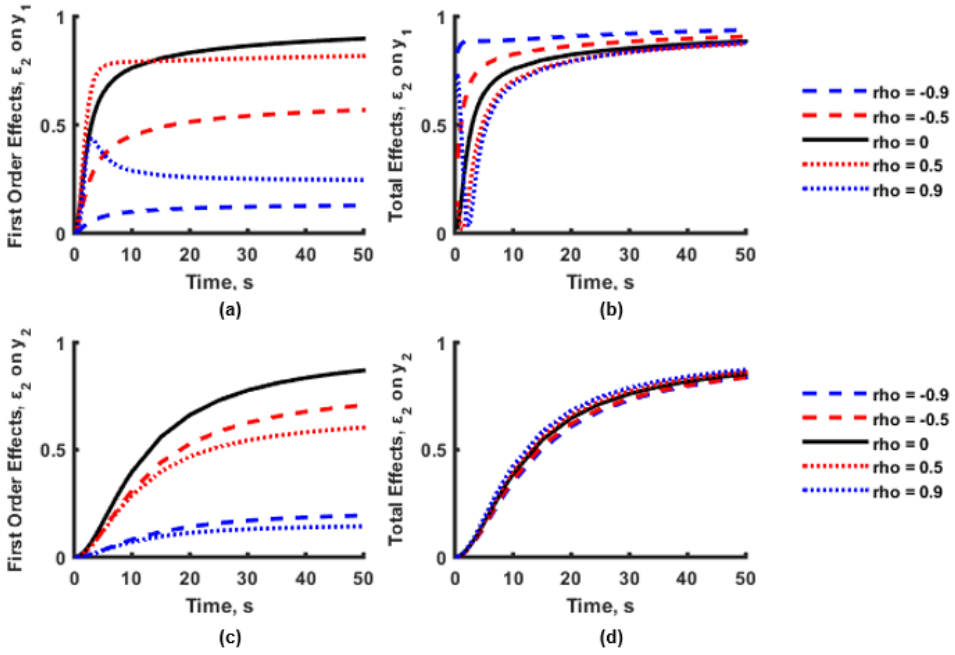

Figure 7. Effect of ε_1 and ε_2 correlation on the sensitivities of y_1 to ε_2 (a-b) and y_2 to ε_2 (c-d)

The effects observed with positive correlation in Figs. 7a-b are not seen in the negative correlation cases since the uncertainty in y_1 ncreases over the entire time history. Likewise, the prediction uncertainty of y_2 grew through time for both positive and negative correlation cases and the summation criterion of $\Sigma S_{d,1} \leq 1$ for the first-order indices and $\Sigma S_{d,T} \geq 1$ for the total effects are maintained in Figs. 7c-d. Furthermore, differences between +/- 0.5 and +/- 0.9 on the in Fig. 7c for first-order effects of y_2 only become apparent at later time instances since ε_1 has negligible effects on y_2 at any given time instant however those effects compound through the coupled iterations.

Upon review of the sensitivity convergence rates for this simple example, the first-order indices of both y_1 and y_2 on average converged in 250 iterations using a Sobol' sequence at all time-instances for all parameters. However, the total effect indices converged in approximately 800 iterations from computing conditional expectation estimates in D-1 rather than d. The convergence rates were no different for the independent or correlated variables when a Sobol' sequence was used. Thererfore, the convergence of the ISK-GSA sensitivity indices with Sobol' sequences is solely dependent on the number of parameters being considered. The comparison of ISK-GSA convergence rates with a Sobol' sequence in higher dimensions will occur in Section IV in the aerothermal coupling application problem.

IV. Application: Aerothermal Coupling

A global sensitivity analysis is performed on coupled aerothermal models to quantify the significance of previously calibrated coupled model errors and uncertainty on aerodynamic heating and heat transfer predictions through time.

A. Aerothermal Model Calibration

Building off of related Bayesian model calibration work by the authors [26–28], the aerodynamic heat flux Q is predicted by Eckert's reference temperature method [29] is coupled with the one-dimensional heat balance equation to predict the structural temperature T_{struct} and wall temperature T_w of a panel on a hypersonic vehicle upstream of an oblique shock.

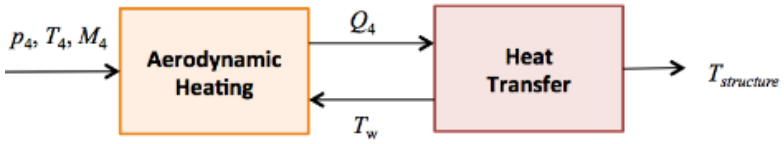

Figure 8. Aerothermal coupling

Aerodynamic heating errors $\delta_{Q,t}$ and heat transfer errors $\delta_{T,t}$ propagate through each iteration and are functions of the changing model inputs according to Eqs. (19) and (20). Here, model error parameters $\boldsymbol{X} = [\, c_0, c_1, d_0, d_1]$ are the only sources of uncertainty considered in order to isolate the effects of the coupled models, their errors, and post-calibration correlation among model error parameters on model output sensitivities through time.

$$\delta_{Q,t}(T_{w,t-1}) = c_0 + c_1 \frac{T_{w,t-1} - T_{w,0}}{T_4} \tag{19}$$

$$\delta_{T,t}(Q_{4,t}) = (d_0 + d_1 Q_{4,t})\Delta t \tag{20}$$

Based off of aerothermal tests conducted in the NASA Langley HTT tunnel [2], the reported heat flux measurements at $t = 0$ shown in Fig. 9 were used to construct a 3 second temperature history at a rates of $\Delta t = 0.05$s (20 samples per second). Measurement noise was assumed to be zero-mean Gaussian with and a standard deviation of 1K. This temperature history was used to calibrate the coupled heat flux and temperature predictions through time and the prior and posterior predictions with 95% confidence bounds are shown in Fig. 9a and 9b, respectively. The calibration was completed using 10^3 slice samples [30] and the posterior correlation among $\boldsymbol{X} = [\, c_0, c_1, d_0, d_1]$ is found in in Eq. (21).

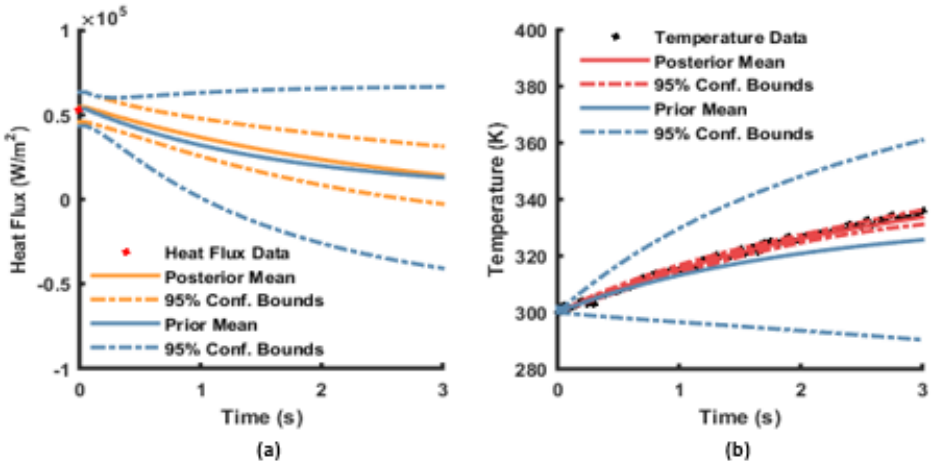

Figure 9. Prior and posterior heat flux (a) and temperature (b) predictions

$$\rho_X = \begin{bmatrix} 1 & -0.29 & -0.42 & 0.02 \\ -0.29 & 1 & -0.54 & 0.10 \\ -0.42 & -0.54 & 1 & -0.59 \\ 0.02 & 0.10 & -0.59 & 1 \end{bmatrix} \tag{21}$$

The joint prior and posterior model error distributions are compared in Fig. 10 at t = 0s and t = 3s where it is seen that model error uncertainty is reduced with calibration but strong correlation is present between both prior and posterior model errors at t = 3s. For example, Fig. 10a shows that at t = 0s the prior correlation between δ_Q, and δ_T is zero and grows to -0.9 in Fig. 10b through model interactions. In comparison, the posterior correlation between δ_Q, and δ_T is -0.6 in Fig. 10a solely from parameter correlations at t = 0s and is -0.95 at t =3s in Fig. 10b. The progression of both the prior and posterior model error correlations through time is shown in Fig. 11.

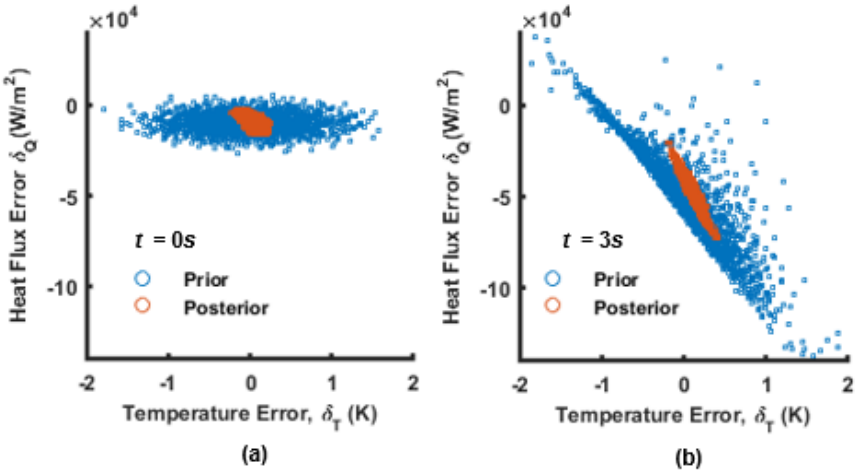

Figure 10. Joint prior and posterior distributions for δ_Q, and δ_T at (a) t = 0s and (b) t = 3s

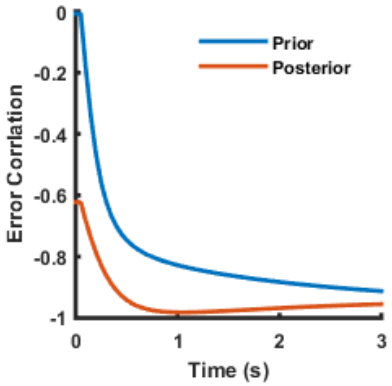

Figure 11. Prior and posterior correlation between δ_Q and δ_T

B. Aerothermal Sensitivities Through Time using Generalized ISK-GSA

Understanding the complex interactions between models, errors, and calibrated parameters from Section IV.A leads to conducting a thorough global sensitivity analysis of the calibrated aerothermal models. The pre-calibration sensitivity estimates of heat flux and temperature to δ_Q and δ_T were performed using generalized ISK-GSA with Sobol' sequences. Figure 12 shows the sensitivity convergences observed during a prior sensitivity analysis using the generalized ISK-GSA method with Sobol' sequences compared to latin-hypercube design of the input space. Similar to the examples in Section II and III, the first-order effects converged using fewer model evaluations than the total effects. Furthermore, the Sobol' sequence of the input space led to faster convergence of the prior first-order sensitivities, where the first-order effects required approximately 600 iterations to satisfy the convergence criteria (<0.1% difference between tests occurring at every 10^{th} iteration) compared to the 1300 iterations requires by the LHS design. It can be seen that neither the total effects from the Sobol' index nor the LHS design converge in 2000 iterations for this 4-dimensional problem.

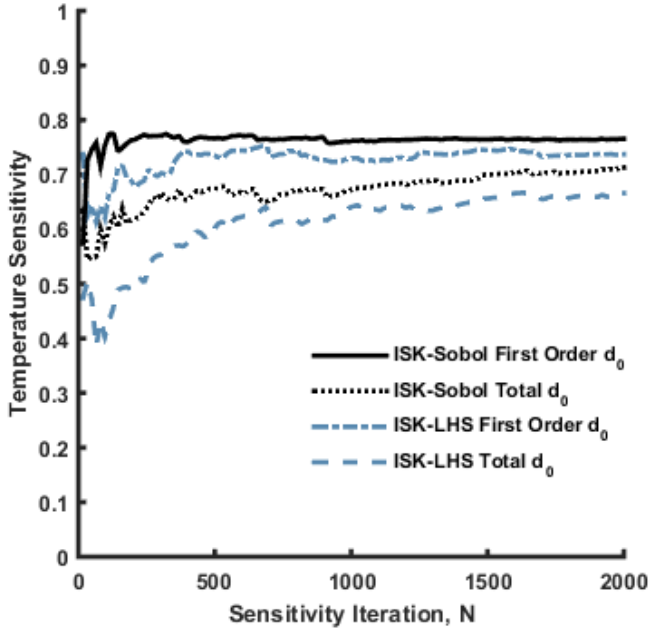

Figure 12. Convergence of prior sensitivities of temperature to d_0 at t = 3s using latin-hypercube and Sobol' sequences

The pre-calibration sensitivity estimates of heat flux and temperature to δ_Q and δ_T were performed using ISK-GSA with Sobol' sequences. The post-calibration sensitivity analysis was performed using the last 4000 posterior samples

from the slice-sampling calibration algorithm after observing the total effects convergence shown in Fig. 12. The generalized ISK-GSA method allows analyzing the sensitivities of both prior and posterior heat flux and temperature predictions to the correlated model errors δ_Q, and δ_T through time.

The prior and posterior heat flux sensitivities are shown in Fig. 13 where, unlike the example in Section III, significant parameter interactions occur within heat flux model which is indicated by the prior total effects in Fig. 13b being greater than the first-order effects in Fig. 13a. The prior first-order effects of δ_T on heat flux are close to zero at t = 0s and increase through time due to strong negative correlation between δ_Q and δ_T shown in Fig. 11.

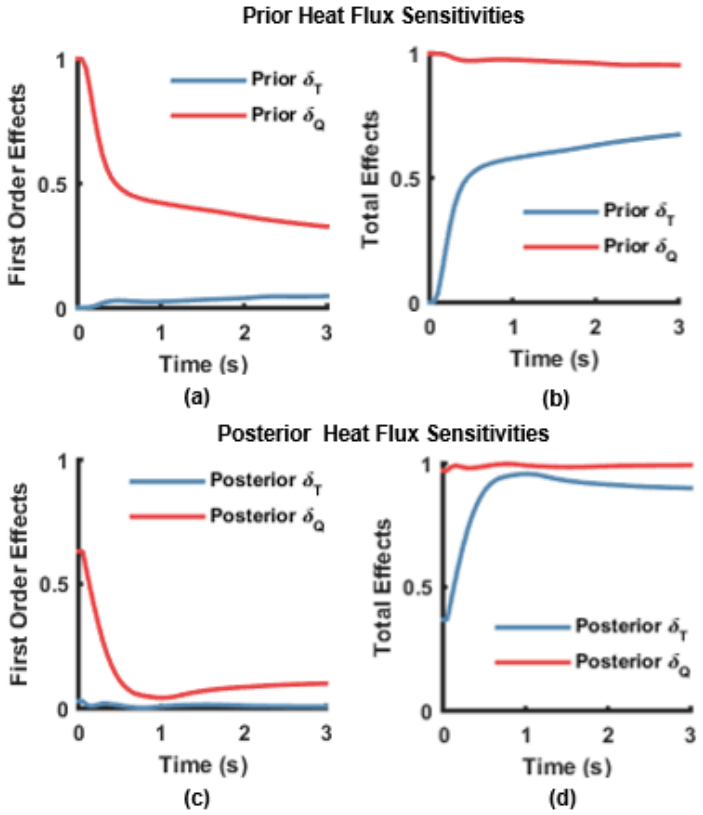

Figure 13. Prior (a-b) and posterior (c-d) heat flux sensitivities through time

In the posterior heat flux sensitivities in Fig. 13c-d, however, the posterior correlation observed between δ_Q and δ_T of -0.6 at t = 0 reduces the first-order effect of δ_Q from 1 (in Fig. 13a) to 0.6 (in Fig. 13b). The posterior first-order effects of δ_Q through time closely mirror the posterior correlation between δ_Q and δ_T in Fig. 11. Again, significant model interactions and the strong negative correlation between δ_Q and δ_T lead to the increase between posterior first-order and total effects of δ_Q and δ_T on heat flux.

The prior temperature sensitivities in Fig 14 show that temperature model is less influenced by model interactions through time since their sums are close to 1 in Fig. 14a-b. In the posterior sensitivities, however, the correlation between model errors at t = 0 moves the sensitivity of δ_Q from 0 in Fig. 14a to 0.45 in Fig. 14c. In the total effects, however, the sensitivity of temperature to δ_T experiences the shift from 1 in Fig. 14b to 0.55 in Fig. 14d. Because of this, the posterior first-order effects in Fig. 14c are greater than the total effects in Fig. 14d. This phenomenon was also observed in Section III in the time-dependent example from positive correlations, which is explored further in Fig. 15 that shows the prior and posterior correlations through time between the temperature predictions and the model errors. Similar to the example in Section III, the temperature prediction and model errors exhibit positive correlations that lead to the posterior temperature sensitivities observed in Fig. 14. Understanding the effect of positive correlation between temperature with δ_Q shown in Fig. 15a and δ_T shown in Fig. 15b along with the negative correlation through time between δ_Q and δ_T from Fig. 11 warrants further investigation.

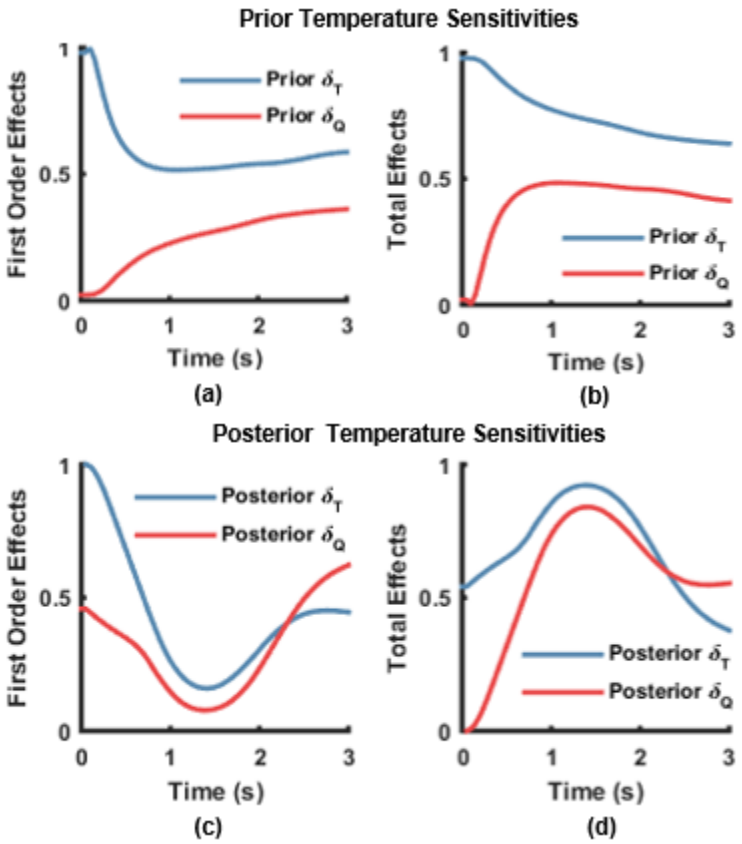

Figure 14. Prior (a-b) and posterior (c-d) temperature sensitivities through time

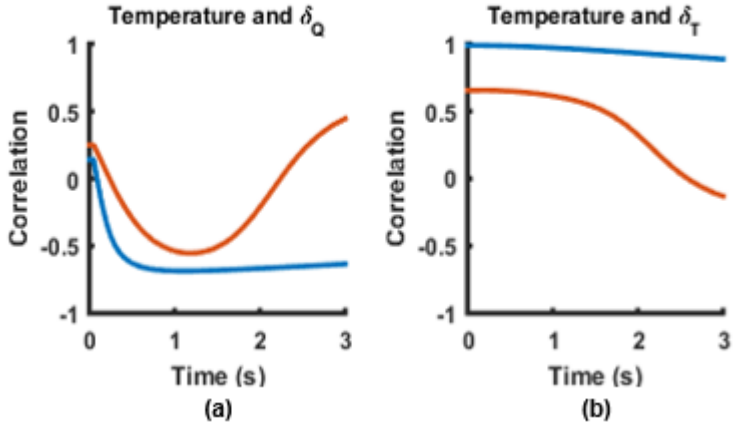

Figure 15. Prior and posterior temperature correlation to (a) δ_Q and (b) δ_T

The comparison between the temperature and heat flux posterior sensitivity convergences to parameter d_0 is shown in Fig. 16. The sensitivity estimates in Fig. 16 were obtained using the last 4000 posterior samples from the slice sampling algorithm and do not follow a Sobol' sequence. First, the total effects of d_0 are higher than the first-order effects indicating that the correlation between d_0 and the other discrepancy parameters is significant at this time instant (t = 3s) for both heat flux and temperature predictions. Second, the lack of a Sobol' sequence within the correlated posterior samples prolongs convergence. Optimizing convergence of the posterior sensitivity estimate by selecting the samples most closely resembling a Sobol' sequence is the subject of future work.

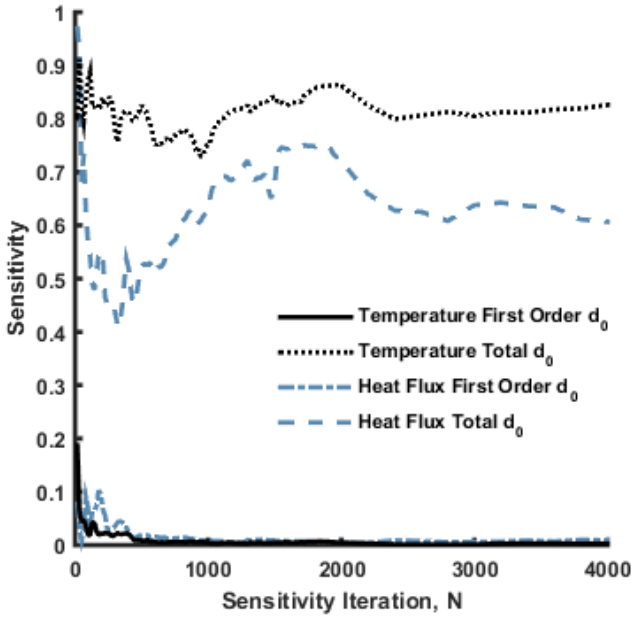

Figure 16. Convergence of posterior sensitivities of temperature and heat flux to d_0 at t = 3s

V. Summary and Future Work

This research has demonstrated increased efficiency in global sensitivity analysis computations by pairing quasi-random number generators with the ISK-GSA methodology. Furthermore, it extended the capability of global sensitivity analysis to correlated quantities by generalizing the ISK-GSA method. Summary of conclusions drawn from this paper are as follows:

1) When paired with quasi-random sequences, the ISK-GSA sensitivity estimate asymptotically converges to the true sensitivity. Therefore, a sensitivity convergence criterion can be used to minimize the number of model evaluations needed for pre-calibration global sensitivity analysis.
2) The ISK-GSA method was generalized for correlated quantites. This development made posterior sensitivity analysis more efficient by allowing use of correlated posterior samples and model outputs obtained from calibration.
3) The generalized ISK-GSA method led to a broader analysis of sensitivity in coupled, time-dependent analyses where first-order and total effects are influenced by both parameter correlation, model errors, and model interactions through time. For example, parameter correlation is important in early time instances while model coupling and interaction effects become more significant through time.
4) For the simplified time-dependent example, negative correlations between model errors maintained the summation criteria for first-order and total effects, however, positive correlations did not early in the analysis from t = 0 to 5 seconds.
5) For the coupled aerothermal problem, the generalized ISK-GSA methodology was applied. It was shown that the prior sensitivity convergences using a Sobol' sequence were asymptotic, however, the posterior convergences using the last 4000 posterior samples did not converge asymptotically.

Building off this effort, the effects that positive correlations among the coupled aerothermal model parameters and errors have on the sensitivities that were estimated by the generalized ISK-GSA method need to be investigated further. Also, the improvement in posterior sensitivity convergences by sequentially selecting the available posterior samples that most closely align with the Sobol' sequence will be tested.

Acknowledgments

This research is sponsored by the National Defense Science and Engineering Graduate (NDSEG) fellowship and the Air Force Office of Scientific Research (AFOSR) Computational Mathematics and Structural Mechanics Programs.

References

[1] Sankararaman, S., "Uncertainty Quantification and Integration," Vanderbilt University, Nashville, TN, 2012.

[2] Glass, C. E., and Hunt, L. R., "Aerothermal tests of spherical dome protuberances on a flat plate at a Mach number of 6.5," NASA TP-2631, 1986.

[3] McNamara, J. J., Friedmann, P. P., Powell, K. G., Thuruthimattam, B. J., and Bartels, R. E., "Aeroelastic and Aerothermoelastic Behavior in Hypersonic Flow," *AIAA Journal*, Vol. 46, No. 10, 2008, pp. 2591–2610. doi: 10.2514/1.36711

[4] Culler, A. J., and McNamara, J. J., "Studies on fluid-thermal structural coupling for aerothermoelasticity in hypersonic flow," *AIAA Journal*, Vol. 48, No. 8, 2010, pp. 1721–1738. doi: 10.2514/1.J050193

[5] Thornton, E. A., and Dechaumphai, P., "Coupled flow, thermal, and structural analysis of aerodynamically heated panels," *Journal of Aircraft*, Vol. 25, No. 11, 1988, pp. 1052–1059. doi: 10.2514/3.45702

[6] Kontinos, D., "Coupled Thermal Analysis Method with Application to Metallic Thermal Protection Panels," *Journal of Thermophysics and Heat Transfer*, Vol. 11, No. 2, Apr. 1997, pp. 173–181. doi: 10.2514/2.6249

[7] Blevins, R. D., Bofilios, D., Holehouse, I., Hwa, V. W., Tratt, M. D., Laganelli, A. L., Pozefsky, P., and Pierucci, M., "Thermo-Vibro-Acoustic Loads and Fatigue of Hypersonic Flight Vehicle Structure," AFRL-RB-WP-TR-2009-3139, 2009.

[8] Blevins, R. D., Holehouse, I., and Wentz, K. R., "Thermoacoustic loads and fatigue of hypersonic vehicle skin panels," *Journal of Aircraft*, Vol. 30, No. 6, Nov. 1993, pp. 971–978. doi: 10.2514/3.46441

[9] Culler, A. J., "Coupled fluid-thermal-structural modeling and analysis of hypersonic flight vehicle structures," The Ohio State University, Columbus, OH, United States, 2010.

[10] Falkiewicz, N., "Enhanced Modal Solutions for Structural Dynamics in Aerothermoelastic Analysis," *Aerospace*, AIAA 2011-1963, Apr. 2011.

[11] Lamorte, N., "Uncertainty Propagation in Hypersonic Vehicle Aerothermoelastic Analysis," 2013.

[12] Lamorte, N., Glaz, B., Friedmann, P. P., Culler, A. J., Crowell, A. R., and Mcnamara, J. J., "Uncertainty Propagation in Hypersonic Aerothermoelastic Analysis," *51st AIAA/ASME/ASCE/AHS/ASC Structures, Structural Dynamics, and Materials and Co-located Conferences*, AIAA 2010-2964, Apr. 2010.

[13] Culler, A. J., and Mcnamara, J. J., "Fluid-thermal-structural modeling and analysis of hypersonic structures under combined loading," *52nd AIAA/ASME/ASCE/AHS/ASC Structures, Structural Dynamics, and Materials and Co-located Conferences*, AIAA 2011-1965, Apr. 2011.

[14] Mahadevan, S., and Liang, B., "Error and Uncertainty Quantification and Sensitivity Analysis in Mechanics Computational Models," *International Journal for Uncertainty Quantification*, Vol. 1, No. 2, 2011, pp. 147–161. doi: 10.1615/IntJUncertaintyQuantification.v1.i2.30

[15] Saltelli, A., Ratto, M., Andres, T., Campolongo, F., Cariboni, J., Gatelli, D., Saisana, M., and Tarantola, S., *Global Sensitivity Analysis: The Primer*, 1st ed. Wiley-Interscience: Hoboken, NJ, 2008.

[16] Ratto, M., Pagano, A., and Young, P., "State Dependent Parameter metamodelling and sensitivity analysis," *Computer Physics Communications*, Vol. 177, No. 11, 2007, pp. 863–876. doi: 10.1016/j.cpc.2007.07.011

[17] Cukier, R. I., Fortuin, C. M., Shuler, K. E., Petschek, A. G., and Schaibly, J. H., "Study of the sensitivity of coupled reaction systems to uncertainties in rate coefficients. I Theory," *Journal of Chemical Physics*, Vol. 59, No. 8, 1973, pp. 3873–3878. doi: 10.1063/1.1680571

[18] Lamorte, N., and Friedmann, P. P., "Uncertainty Propagation in Integrated Airframe-Propulsion System

Analysis for Hypersonic Vehicles," *17th AIAA International Space Planes and Hypersonic Systems and Technologies Conference*, AIAA 2011-2394, 2011.

[19] Hosder, S., Walters, R. W., and Balch, M., "Efficient uncertainty quantification applied to the aeroelastic analysis of a transonic wing," *46th AIAA Aerospace Sciences Meeting and Exhibit*, AIAA 2008-729, 2008.

[20] Doksum, K., and Samarov, A., "Nonparametric Estimation of Global Functionals and a Measure of the Explanatory Power of Covariates in Regression," *The Annals of Statistics*, Vol. 23, No. 5, 1995, pp. 1443–1473.

[21] Sparkman, D., Garza, J., Millwater, H., and Smarslok, B., "Importance Sampling-based Post-processing Method for Global Sensitivity Analysis," *15th*.

[22] Camberos, J. A., Josyula, E., and Lambe, L. A., "Quasi-Random Monte Carlo Integration for Computing Dissociation Rates," *AIAA Termophysics Conference*, AIAA 2007-4260, Jun. 2007.

[23] Sobol, I. M., "Global sensitivity indices for nonlinear mathematical models and their Monte Carlo estimates," *Mathematics and Computers in Simulation*, Vol. 55, No. 1–3, 2001, pp. 271–280. doi: 10.1016/S0378-4754(00)00270-6

[24] Saltelli, A., Annoni, P., Azzini, I., Campolongo, F., Ratto, M., and Tarantola, S., "Variance based sensitivity analysis of model output. Design and estimator for the total sensitivity index," *Computer Physics Communications*, Vol. 181, No. 2, 2010, pp. 259–270. doi: 10.1016/j.cpc.2009.09.018

[25] Sobol, I. M., "Quasi-Monte Carlo methods," *Progress in Nuclear Energy*, Vol. 24, No. 1–3, Jan. 1990, pp. 55–61. doi: 10.1016/0149-1970(90)90022-W

[26] DeCarlo, E. C., Mahadevan, S., and Smarslok, B. P., "Bayesian Calibration of Coupled Aerothermal Models Using Time-Dependent Data," *16th AIAA Non-Deterministic Approaches Conference at AIAA SciTech*, AIAA 2014-0123, Jan. 2014.

[27] DeCarlo, E. C., Mahadevan, S., and Smarslok, B. P., "Bayesian Calibration of Aerothermal Models for Hypersonic Air Vehicles," *54th AIAA/ASME/ASCE/AHS/ASC Structures, Structural Dynamics, and Materials and Co-located Conferences*, AIAA 2013-1683, Apr. 2013.

[28] DeCarlo, E. C., Smarslok, B. P., and Mahadevan, S., "Segmented Bayesian Calibration of Multidisciplinary Models," *AIAA Journal*, Vol. 54, No. 9, 2016, pp. 1–15. doi: 10.2514/1.J054960

[29] Eckert, E. R. G., "Engineering Relations for Heat Transfer and Friction in High-Velocity Laminar and Turbulent Boundary-Layer Flow over Surfaces with Contstant Pressure and Temperature," *Transactions of the ASME*, Vol. 78, No. 6, 1956, pp. 1273–1283.

[30] Neal, R. M., "Slice sampling," *The Annals of Statistics*, Vol. 31, No. 3, 2003, pp. 705–767. doi: 10.1214/aos/1056562461